

Electrical properties and temperature sensitivity of Li/Fe-modified NiO-based ceramics as NTC thermistors

Jiaxi Wang¹ · Hong Zhang^{1,2} · Xiang Sun¹ · Ya Liu¹ · Zhicheng Li^{1,2}

Received: 31 May 2016 / Accepted: 9 July 2016 / Published online: 15 July 2016
© Springer Science+Business Media New York 2016

Abstract To develop a new system of negative temperature coefficient (NTC) thermistors, Li/Fe-modified NiO-based ceramics, $\text{Ni}_{1-x-y}\text{Li}_x\text{Fe}_y\text{O}$ (x : 0.00–0.08; y : 0.00–0.06), were prepared through a wet chemical process. The phase component and microstructure of the ceramics were analyzed respectively by using X-ray diffraction and electron microscopy, and the related electrical properties were investigated by resistance–temperature measurement and complex impedance analysis. The results show that all the ceramics have the cubic-type NiO crystalline structure and show typical NTC characteristic. The NTC material constant $B_{25/85}$ ranges from 335 to 5169 K and room-temperature resistivity $\ln\rho_{25}$ ranges from 3.97 Ω cm to 1.99 M Ω cm, when the ceramics were modified by various contents of Li- and Fe-ions. The conduction mechanisms combining the electron-hopping model and band conduction are supposed for the NTC effect in the Li/Fe-modified NiO ceramics.

1 Introduction

Negative temperature coefficient (NTC) thermistors, whose resistivities obviously decrease with the temperature increasing, act as a key element in various electrical/electronic devices and are widely applied in the fields such as circuit compensation, aerospace, solar cells, automotive temperature measurement and control applications.

Traditional NTC ceramic thermistors with the spinel structure are always composed of multiple transition-metal oxides, for instance, Mn–Ni–O, Mn–Ni–Cu–O and Mn–Co–Ni–O systems [1]. Those spinel-type thermistors limit the application temperatures below 200 °C for the relaxation of crystalline structure at higher temperatures [2]. Numerous work have tried to improve the electrical property and ageing resistance of the spinel-type thermistors by cation doping [3, 4] and microstructure modification [5], etc.

On the other hand, the conduction in the spinel manganese ceramics is generally accepted as an electron hopping mechanism taking place between the Mn^{3+} and Mn^{4+} cations locating on the octahedral sites [6, 7]. The exact oxidation states of the Mn cations in the spinel structure obviously depend on the temperature and oxygen partial pressure during sintering, so those ceramics typically exhibit a considerably different in resistivity for a minor change of oxygen partial pressure during sintering or annealing [8, 9]. The controllable resistivity, suitable material constant B , high stability and good accuracy of a NTC thermistor are always required for the real applications. Therefore, to develop new types of NTC thermistors should be of importance and interesting, and attracted much attention in past years [10–15]. Meanwhile, the NTC thermistors based on simple semiconducting oxides such as SnO_2 and CuO show obvious merits such as adjustable resistivity by doping, suitable material constant B by element substitution, high stability and low cost, etc. [16–19].

NiO is one kind of semiconductor with a band gap of about 3.50 eV [20], its electrical properties can be improved by doping with various dopants. The related electrical properties are strongly dependent on the dopant type and doping content. The NiO-based materials have been intensively studied for various applications such as

✉ Zhicheng Li
zhchli@csu.edu.cn

¹ School of Materials Science and Engineering, Central South University, Changsha 410083, China

² State Key Laboratory of Powder Metallurgy, Central South University, Changsha 410083, China

dielectric, magnetic, gas sensors, thermoelectric, catalyst [21–26], and electrodes for lithium-ion batteries or supercapacitors [27]. However, little work has been done to investigate its temperature sensitivity such as NTC feature. To achieve NiO-based NTC thermistors with suitable room-temperature resistivity (ρ_{25}) and B values, Li/Fe modified NiO ceramics were prepared in present work. The related electrical properties and conduction mechanisms were investigated by measuring the resistivity-temperature characteristic and analyzing the related complex impedance spectra.

2 Experimental

Li/Fe-modified NiO-based powders ($\text{Ni}_{1-x-y}\text{Li}_x\text{Fe}_y\text{O}$, $x = 0, 0.01, 0.02, 0.03, 0.04, 0.05, 0.06$ and 0.08 ; $y = 0, 0.03, 0.035, 0.04, 0.045, 0.05$ and 0.06) were prepared by a wet chemical process with polyvinyl alcohol (PVA) as a polymeric carrier. Basic nickel carbonate ($\text{NiCO}_3 \cdot 2\text{Ni}(\text{OH})_2 \cdot 4\text{H}_2\text{O}$), lithium carbonate (Li_2CO_3) and ferric citrate ($\text{FeC}_6\text{H}_5\text{O}_7 \cdot n\text{H}_2\text{O}$) were used as the starting materials. The starting materials were weighed, respectively, according to the formula of $\text{Ni}_{1-x-y}\text{Li}_x\text{Fe}_y\text{O}$ in each batch. $\text{NiCO}_3 \cdot 2\text{Ni}(\text{OH})_2 \cdot 4\text{H}_2\text{O}$ and Li_2CO_3 were dissolved into diluent nitric acid solution, and $\text{FeC}_6\text{H}_5\text{O}_7 \cdot n\text{H}_2\text{O}$ was dissolved into hot deionized water. Then the solutions were mixed together, and an appropriate amount of PVA was added into the mixed solution for the effective preparation of mixed oxides. The mixed solution was heated with stirring and dried to get the precursors. After calcining at 850°C for 5 h in air, the powders were pressed into pellets of 12 mm diameter and 3.5 mm thickness, and the pellets were sintered at 1200°C for 40 min. The sintered ceramics were polished into a thickness of about 2 mm. The silver paste was painted on both parallel sides of the ceramics and fired at 600°C for 5 min to make the electrodes.

The temperature dependence of resistivity (R – T) of the samples was tested by using a resistance–temperature measurement system (ZWX-C, China) in the direct current (DC) condition, at temperatures ranged in 25 – 300°C . An electrochemical measurement system (Gamry Reference 600, USA) was used to measure the alternating current (AC) impedance in the temperature range of 25 – 300°C , in the testing frequency from 0.1 Hz to 1 MHz. Phase identification of the ceramics was performed by using an X-ray diffractometer with Cu-K_α radiation ($\lambda = 0.154056$ nm) (Rigaku D/max 2500, Japan). For the microstructure observation by scanning electron microscope (SEM, FEI Quanta 200), the sintered pellets were broken into pieces, and the fracture surface morphology was observed. For the transmission electron microscopy (TEM, FEI Tecnai G² F20) observation, the ceramic was grounded into powder

and was dispersed into ethanol, and a drop of the suspension was transferred onto a Cu-grid with holey carbon foil. The bright-field images and selected area electron diffraction (SAED) patterns were obtained. The X-ray photoelectron spectra (ESCALAB 250X1, Thermo Fisher, USA) were recorded to evaluate the valence states of the ceramics. The XPS profiles of the samples were obtained using an Al K_α X-rays source. The C1 s peak was used as the reference.

3 Results and discussion

3.1 Phase identification

Figure 1 shows the X-ray diffraction (XRD) patterns of the as-sintered ceramics of NiO, $\text{Ni}_{0.96}\text{Li}_{0.04}\text{O}$ and $\text{Ni}_{0.91}\text{Li}_{0.04}\text{Fe}_{0.05}\text{O}$. By analyzed with a Jade6 + pdf2004 program, all the ceramics are detected to have a cubic lattice with a space group of $Fm\bar{3}m$ (225). The lattice parameters of Li/Fe-doped NiO ceramics are little different from the ones of the reference NiO (PDF no. 47-1049, $a = 4.177$ Å) and the as-sintered pure NiO, e.g., $a = 4.1246$ Å for pure NiO, $a = 4.1505$ Å for $\text{Ni}_{0.96}\text{Li}_{0.04}\text{O}$, and $a = 4.1799$ Å for $\text{Ni}_{0.91}\text{Li}_{0.04}\text{Fe}_{0.05}\text{O}$. The lattice parameter difference should result from the formation of lattice vacancies and/or the solid solution for the Li- and Fe-ions substituted into NiO lattice. The lattice vacancies might occur in the pure NiO ceramics during sintering for the oxygen atmosphere was not suitable inside the muffle furnace, resulting in the smaller lattice parameter. When the Li- and Fe-ions substitute into the NiO crystal lattice, for the larger ionic radii of Li^+ ion (Li^+ : 0.74 Å), Fe^{2+} (Fe^{2+} : 0.78 Å) that the Ni^{2+} ion (Ni^{2+} : 0.70 Å) [28], the lattice parameter increased.

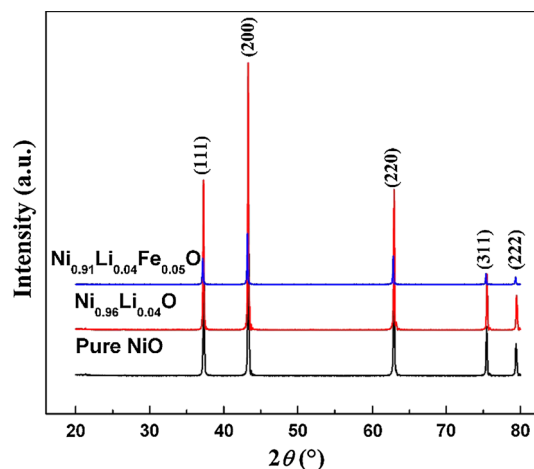


Fig. 1 XRD patterns of the as-sintered ceramics of NiO, $\text{Ni}_{0.96}\text{Li}_{0.04}\text{O}$ and $\text{Ni}_{0.91}\text{Li}_{0.04}\text{Fe}_{0.05}\text{O}$

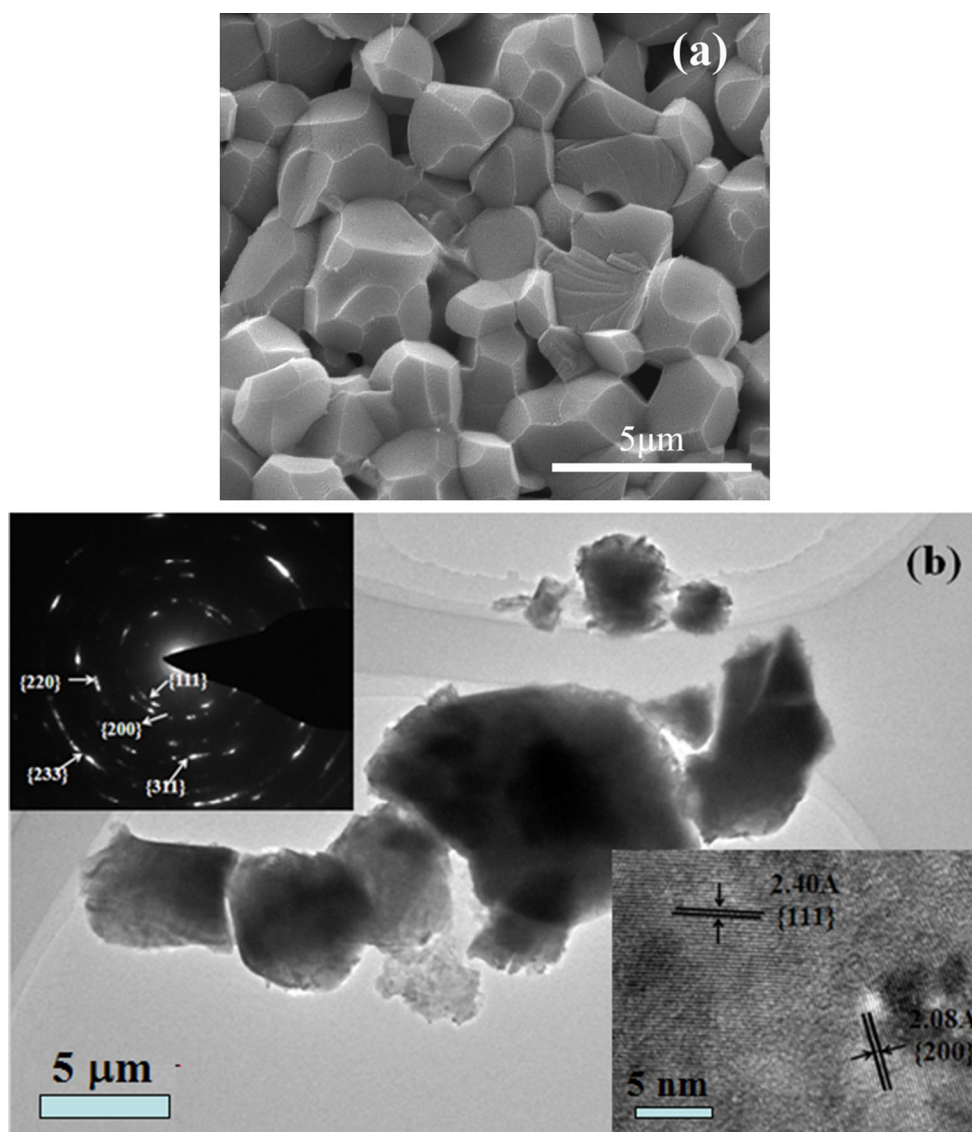


Fig. 2 Microstructure investigations of as-sintered $\text{Ni}_{0.91}\text{Li}_{0.04}\text{Fe}_{0.05}\text{O}$ ceramic, **a** SEM image, **b** TEM observation with the *inset* SAED pattern and HRTEM image

Figure 2 shows the microstructure investigations of an as-sintered $\text{Ni}_{0.91}\text{Li}_{0.04}\text{Fe}_{0.05}\text{O}$ ceramic. Figure 2a is an SEM image of the fracture surface. Grains are distinctly uniform and densely packed together. The mean grain size is about $3\ \mu\text{m}$. Figure 2b shows the TEM investigations, including a bright-field image, related SAED pattern (upper-left inset) and down-right inset high-resolution TEM image. By analyzing the SAED pattern, (111), (200), (220), (311) and (233) can be indexed based on cubic NiO. The corresponding lattice spacing of 2.40 and 2.08 Å as marked in the high-resolution TEM image are in agreement with the ones of {111} and {200} as obtained by the SAED analysis, respectively. Both the indexed SAED pattern and the HRTEM image analysis reveal the cubic type of the

NiO-based ceramic, and are in agreement with the XRD results mentioned in Fig. 1.

To detect the possible valence-variable ions, XPS spectrum of $\text{Ni}_{0.91}\text{Li}_{0.04}\text{Fe}_{0.05}\text{O}$ ceramic was recorded and analyzed as showed in Fig. 3. The *inset* is the narrow spectra corresponding to the Ni-ions. The results show that there are Ni^{3+} and Ni^{2+} ions coexisting in the ceramics.

3.2 Electrical properties

As a semiconductor, its conductivity can be effectively adjusted by doping with various dopants [22, 29]. In this work, Li-doped NiO ceramics have been made. The room-temperature resistivities ρ_{25} of the single Li-doped NiO

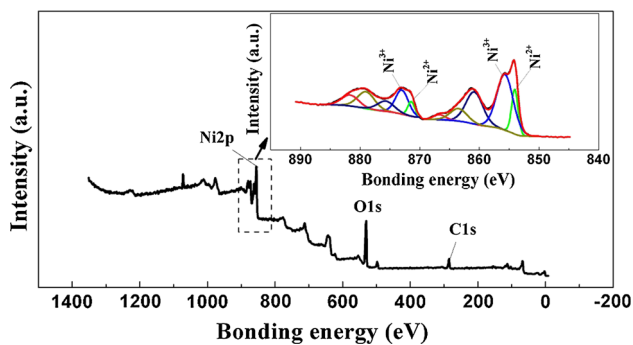


Fig. 3 XPS spectrum of the Ni_{0.91}Li_{0.04}Fe_{0.05}O ceramic, the inset is the narrow spectra corresponding to the Ni-ions

ceramics, Ni_{1-x}Li_xO, are 10.63, 7.81, 4.97, 3.97 and 4.20 Ω cm for x are 0.01, 0.02, 0.03, 0.04 and 0.05, respectively. These indicate that acceptor Li⁺ is an effective semiconducting ion for NiO. Although NiO is one kind of semiconductor with a band gap of about 3.50 eV, a stoichiometric NiO was reported to be a Mott–Hubbard insulator with the conductivity at room temperature less than 10⁻¹³ S cm⁻¹ [30], its conductivities are closely dependant on the sintering condition or doping with monovalent ions such as Li⁺ [31]. The Li⁺ ions substituted into the NiO lattice may act as the acceptors, resulting in the occurrence of electron holes and the acceptor level locating near the valence-band top, p-type semiconductor formed, the electric conduction follows the band conduction mechanism. At the same time, the Ni²⁺ ions can be enhanced to the Ni³⁺ state, which is the lost electron filling a state in the oxygen 2p valence band. So the lattice contains Ni²⁺ and Ni³⁺ ionic pair on equivalent sites as shown in Fig. 3, which satisfies the conduction mechanism of polaron hopping [31]. The hopping conduction mechanism will further be investigated by complex impedance spectra in the next section.

Figure 4a presents the temperature dependence of resistivity, in Arrhenius plots, of the Ni_{0.96-y}Li_{0.04}Fe_yO ceramics with various contents of Fe. One can see that all the ceramics have the typical NTC characteristic, and ρ₂₅ increases with the increase of the Fe concentration. The plots of temperature dependence of resistivity are approximately linear and nearly comply with the Arrhenius relationship as showed in Eq. (1).

$$\rho = \rho_0 \exp\left(\frac{E_a}{kT}\right) \tag{1}$$

where, ρ is the resistivity at temperature of T (in Kelvin), ρ₀ is pre-exponential factor, E_a is activation energy of conduction, k is Boltzmann constant. For NTC thermistors, the material constant B is equal to E_a/k and can also be calculated by Eq. (2).

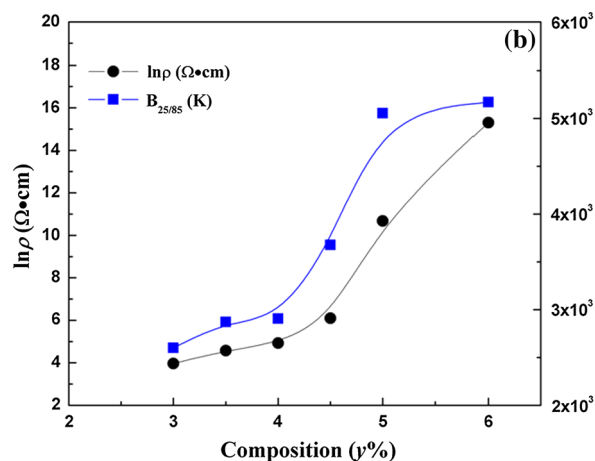
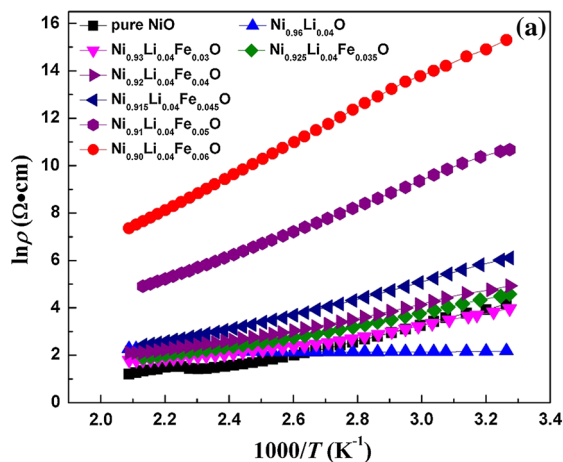


Fig. 4 Electrical properties of Fe-substituted Ni_{0.96}Li_{0.04}O ceramics with various contents of Fe, **a** temperature dependence of resistivity in Arrhenius plots, **b** Fe-concentration dependence of material constants B_{25/85} and room-temperature resistivities ρ₂₅

$$B_{25/85} = \frac{\ln(\rho_{25}/\rho_{85})}{1/T_{25} - 1/T_{85}} \tag{2}$$

where, ρ₂₅ and ρ₈₅ are the resistivities at T₂₅ (25 °C) and T₈₅ (85 °C), respectively. The ρ₂₅ and calculated B_{25/85} of the Ni_{0.96-y}Li_{0.04}Fe_yO ceramics with various Fe-contents are illustrated in Fig. 4b. It shows that both ρ₂₅ and B_{25/85} can be adjusted by changing the Fe-content in Ni_{0.96-y}Li_{0.04}Fe_yO ceramics. The B value reaches up to 5169 K when y is 0.06 in Ni_{0.96-y}Li_{0.04}Fe_yO.

Figure 5 shows the Arrhenius plots of the Ni_{0.95-x}Li_xFe_{0.05}O ceramics with various contents of Li (x = 0.04, 0.05, 0.06, 0.08). One can see that all of the ceramics also show NTC effect. The ρ₂₅ and B_{25/85} of the ceramics are in the ranges of 34.6–2770 Ω cm and 1430–4335 K, respectively, for various Li-contents.

Based on the measurement and analysis as discussed above, the electrical parameters of the Li/Fe modified NiO ceramics are collected and shown in Table 1. One can get

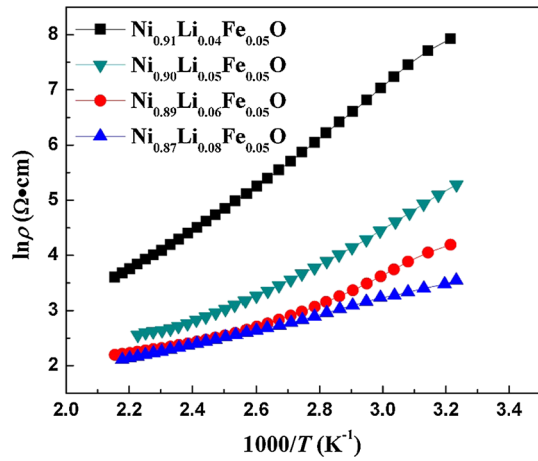


Fig. 5 Temperature dependence of resistivity of $\text{Ni}_{0.95-x}\text{Li}_x\text{Fe}_{0.05}\text{O}$ ceramics with various of Li-contents

Table 1 The room-temperature resistivities (ρ_{25}) and NTC material constants ($B_{25/85}$) of $\text{Ni}_{1-x-y}\text{Li}_x\text{Fe}_y\text{O}$ ceramics with various contents of Li and Fe

Li content, x	Fe content, y	ρ_{25} ($\Omega \text{ cm}$)	$B_{25/85}$ (K)
0.00	0.00	64.14	3217
0.01	0.00	10.63	459
0.02	0.00	7.81	112
0.03	0.00	4.97	733
0.04	0.00	3.97	335
0.05	0.00	4.20	1140
0.04	0.03	40.42	2599
0.04	0.035	97.24	2870
0.04	0.04	117.05	2906
0.04	0.045	445.86	3676
0.04	0.05	2768.69	4334
0.04	0.055	43,367.69	5053
0.04	0.06	1,999,104.72	5169
0.05	0.05	196.96	3391
0.06	0.05	66.33	2628
0.08	0.05	34.63	1429

that the ρ_{25} and $B_{25/85}$ of the Li/Fe doped NiO ceramics can be effectively modified by changing the contents of Fe and Li. As discussed above, moderate Li-doping can improve the conductivity of NiO, however, Fe-doping deteriorates the room-temperature conductivity and increased the conduction activation energy, i.e., NTC B value increases. For the Fe-doping, Fe^{2+} and Fe^{3+} might coexist in the NiO lattice, and the low concentration of Fe-ion should not change the Ni-ion valent state. Because of the larger ionic radius of Fe^{2+} than that of Ni^{2+} ion, lattice distortion occurred for the Fe-substitution, reduced the hopping probability and conduction process, resulting in the higher conduction activation energy. On the other hand, the added

Fe-ions might not entirely substitute into the NiO lattice, and the remanent ones located at the grain surface or grain boundaries. The Fe-ions segregating at the boundary will hinder the mobility of charge carrier across the grain boundary, resulting in the rise of resistivity and $B_{25/85}$.

3.3 Impedance analysis

In order to further investigate the conduction characteristic of the NiO-based ceramics. AC impedance spectroscopy was employed in this work. Figure 6 shows a series of complex impedance spectra (CIS) of the $\text{Ni}_{0.91}\text{Li}_{0.04}\text{Fe}_{0.05}\text{O}$ ceramic at various temperatures. Part of arc at the higher frequency region (left part in the CIS) and an arc at the lower frequency region (right part in the CIS) can be identified in the CIS measured at 30 and 40 °C (see in Fig. 6a). The high-frequency arc gradually decreased and even disappeared when the temperature further rises. And only one arc or part arc can be detected at temperatures above 55 °C (see in Fig. 6b). An equivalent circuit is applied to fit the CIS data (see inset in Fig. 6a), where R_b and R_{gb} represent the resistances from the bulk effect (grain effect) and grain boundary effect, respectively, and CPE_b and CPE_{gb} are constant phase elements from the bulk effect and grain boundary effect, respectively. The impedance response of a constant-phase element (CPE) can be defined as $Z_{\text{CPE}} = 1/((j\omega)^\alpha Q)$ [32]. Here, j is the imaginary unit ($j^2 = -1$) and ω is the angular frequency; Q and α are the CPE parameters which are frequency independent. The parameter α mathematically represents an angle of rotation in the complex plane with respect to the impedance response of an ideal capacitor, and always ranges between 0.5 and 1. The CPE coefficient Q is the combination of properties related to both the surface and the electro-active species, and represents the differential capacitance of the interface when $\alpha = 1$. The equivalent circuit can well fit the CISs, meaning that each CIS originated from both bulk effect (grain effect) and grain boundary effect. The fitting parameters are presented in Table 2. Figure 6c shows the temperature dependence of R_b and R_{gb} . One can see that R_b , R_{gb} and total resistance ($R_b + R_{gb}$) have similar temperature-dependence characteristics, indicating that the bulk effect and grain boundary effect contribute comparably to the NTC effect of the NiO-based ceramics.

To reveal the electrical processes in the ceramics, normalized imaginary impedance (Z''/Z''_{max}) and electrical modulus (M''/M''_{max}) of $\text{Ni}_{0.91}\text{Li}_{0.04}\text{Fe}_{0.05}\text{O}$ at different temperatures were analyzed as shown in Fig. 7. At temperatures below 40 °C, there should have two peaks, one at the middle frequency region representing the grain boundary conduction and another at higher frequency region reflecting the bulk conduction (the latter has only part of peak). At higher temperatures, only the peak

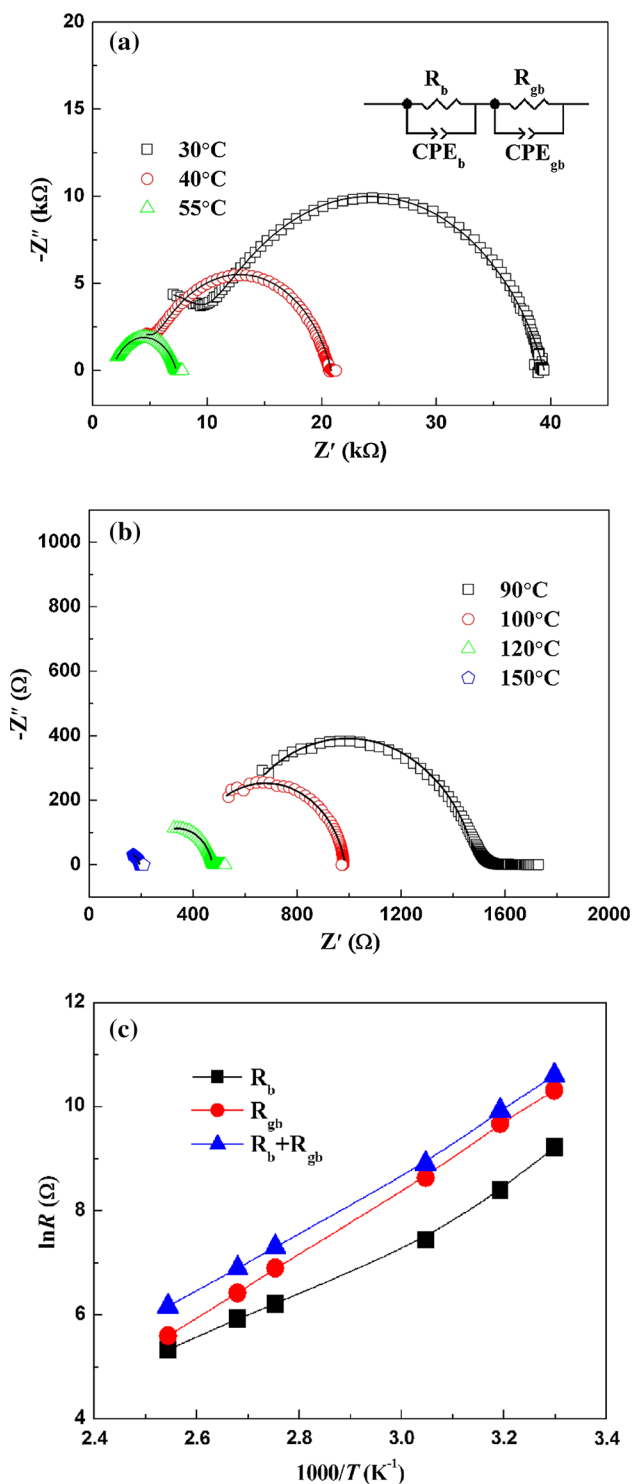


Fig. 6 Complex impedance spectra of $Ni_{0.91}Li_{0.04}Fe_{0.05}O$ ceramic at various temperatures, **a** 30, 40 and 55 °C, and an *inset* equivalent circuit model adopted for fitting the impedance spectra; **b** 90, 100, 120 and 150 °C; **c** Temperature dependence of impedances from bulk effect (R_b), grain boundary effect (R_{gb}) and total resistance ($R_b + R_{gb}$)

Table 2 Fitting parameters of the complex impedance spectra of $Ni_{0.91}Li_{0.04}Fe_{0.05}O$ ceramic at various temperatures

T (°C)	R_b (Ω)	R_{gb} (Ω)	CPE_b		CPE_{gb}	
			Q (nS s 2)	α	Q (nS s 2)	α
30	9998	30,094	0.084	0.855	9.132	0.740
40	4417	15,806	0.087	0.879	6.395	0.769
55	1698	5590	0.089	0.837	8.356	0.760
90	498	991	0.092	0.801	4.183	0.852
100	373	612	0.092	0.798	3.205	0.881
120	206	268	0.093	0.773	3.717	0.890

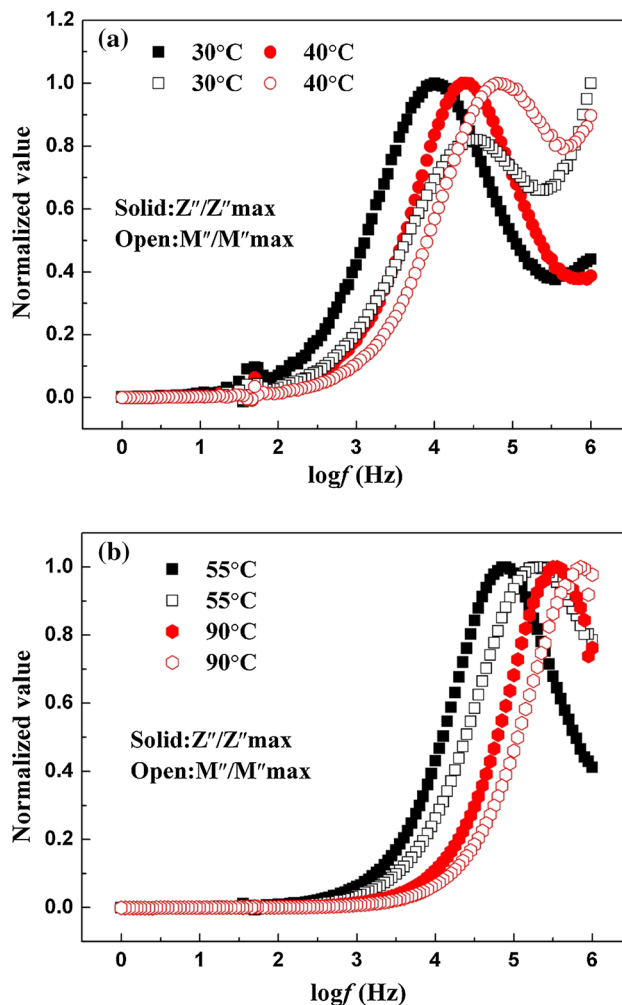


Fig. 7 Comparison of Normalized imaginary part of impedance (Z''/Z''_{max}) and electrical modulus (M''/M''_{max}) of $Ni_{0.91}Li_{0.04}Fe_{0.05}O$ at various temperatures, **a** 30 and 40 °C, **b** 55 and 90 °C

representing the grain boundary effect can be detected. At each temperature, the Z''/Z''_{max} and M''/M''_{max} are mismatch with each other. Usually, the mismatch between $Z''/$

Z''_{\max} and M''/M''_{\max} peaks is considered to be the evidence of localized conduction which is in accordance with the hopping conduction [12]. The electron hopping takes place in the valence-variable ions locating at the same crystallographic positions. It indicates that the thermally activated electron hopping between $\text{Ni}^{3+}/\text{Ni}^{2+}$ pairs could be proposed to be $\text{Ni}^{3+} + \text{Ni}^{2+} \rightarrow \text{Ni}^{2+} + \text{Ni}^{3+}$.

4 Conclusion

Li/Fe modified NiO ceramics, $\text{Ni}_{1-x-y}\text{Li}_y\text{Fe}_x\text{O}$ (x : 0.00–0.08; y : 0.00–0.06), have a cubic phase with space group of $Fm\bar{3}m$ (225) as that of pure NiO. The NiO-based ceramics show a typical NTC effect, in which the material constant B can be widely adjusted by changing the Li content and Fe content. The NTC material constant B value reaches high up to 5169 K when the contents of Li and Fe are $x = 0.04$ and $y = 0.06$, respectively. The adjustable B values and room-temperature resistivities of the NiO-based ceramics modified by Li/Fe ions should be useful for the development of high performance NTC thermistor devices. The conduction of the NiO-based ceramics resulted from both grain effect and grain-boundary effect. The possible conduction mechanisms are proposed to consist of the band conduction and hopping conduction models.

Acknowledgments The authors acknowledge the support of the National Nature Science Foundation of China (No. 51172287) and the Research Funds by the State Key Laboratory of Powder Metallurgy, Central South University, China.

References

1. A. Feteira, J. Am. Ceram. Soc. **92**, 967–983 (2009)
2. A. Feltz, W. Pözl, J. Eur. Ceram. Soc. **20**, 2353–2366 (2000)
3. D. Fang, C. Chen, A.J.A. Winnubst, J. Alloys Compd. **454**, 286–291 (2008)
4. K. Park, I.H. Han, Mater. Sci. Eng. B **119**, 55–60 (2005)
5. R. Ranjan, R. Kumar, B. Behera, R.N.P. Choudhary, Phys. B: Condens. Matter **404**, 3709–3716 (2009)
6. E.D. Macklen, J. Thermistors, J. Phys. Chem. Sol. **47**, 1073–1079 (1986)
7. J. Jung, J. Topfer, J. Murbe, A. Feltz, J. Eur. Ceram. Soc. **6**, 351–359 (1990)
8. P. Fau, J.P. Bonino, J.J. Demai, A. Rousset, Appl. Surf. Sci. **65/66**, 319 (1993)
9. A. Basu, A.W. Brinkman, R. Schmidt, J. Eur. Ceram. Soc. **24**, 1247 (2004)
10. D. Xue, H. Zhang, Y. Li, Y. Liu, Z. Li, J. Mater. Sci.: Mater. Electron. **2**, 1306–1312 (2012)
11. M.A.L. Nobre, S. Lanfredi, Appl. Phys. Lett. **82**, 2284–2286 (2003)
12. J. Wang, H. Zhang, D. Xue, Z. Li, J. Phys. D Appl. Phys. **42**, 235103 (2009)
13. P. Ouyang, H. Zhang, D. Xue, Z. Li, J. Mater. Sci.: Mater. Electron. **24**, 3932–3939 (2013)
14. S. Upadhyay, O. Parkash, D. Kumar, J. Phys. D Appl. Phys. **37**, 1483–1491 (2004)
15. W.T. Chen, F. Sher, N.D. Mathur, C.M. Kavanagh, F.D. Morrison, J.P. Attfield, Chem. Mater. **24**, 199–208 (2012)
16. P. Ouyang, H. Zhang, Y. Zhang, J. Wang, Z. Li, J. Mater. Sci.: Mater. Electron. **26**, 6163–6169 (2015)
17. Y. Zhang, Y. Wu, H. Zhang, W. Chen, G. Wang, Z. Li, J. Mater. Sci.: Mater. Electron. **25**, 5552–5559 (2014)
18. J. Zhang, H. Zhang, B. Yang, Y. Zhang, Z. Li, J. Mater. Sci.: Mater. Electron. **27**(5), 4935–4942 (2016)
19. B. Yang, H. Zhang, J. Zhang, X. Zhang, Z. Li, J. Mater. Sci.: Mater. Electron. **26**, 10151–10158 (2015)
20. Y. Xu, M.A.A. Schoonen, Am. Mineral. **85**, 543–556 (2000)
21. J. Wu, C.W. Nan, Y.H. Lin, Y. Deng, Phys. Rev. Lett. **89**, 217601 (2002)
22. N. Fuschillo, B. Lalevic, B. Leung, Thin Solid Films **24**, 181–192 (1974)
23. W.L. Roth, Phys. Rev. **110**, 1333 (1958)
24. A. Wisitsoraat, A. Tuantranont, E. Comini, G. Sberveglieri, W. Wlodarski, Thin Solid Films **517**, 2775–2780 (2009)
25. W. Shin, N. Murayama, Mater. Lett. **45**, 302–306 (2000)
26. H.J. Gallon, X. Tu, M.V. Twigg, J.C. Whitehead, Appl. Catal. B **106**, 616–620 (2011)
27. Z. Ma, H. Zhang, Y. Zhang, J. Zhang, Z. Li, Electrochim. Acta **176**, 1427–1433 (2015)
28. R.D. Shannon, C.T. Prewitt, Acta Cryst. **B25**, 925–945 (1969)
29. W. Yan, W. Weng, G. Zhang, Z. Sun et al., Appl. Phys. Lett. **92**, 052508 (2008)
30. J. Wu, C.W. Nan, Y.H. Lin, Y. Deng, Phys. Rev. Lett. **89**, 217601 (2000)
31. P. Thongbai, T. Yamwong, S. Maensiri, Mater. Chem. Phys. **123**, 56–61 (2010)
32. X. Dominguez-Benetton, S. Sevda, K. Vanbroekhoven, D. Pant, Chem. Soc. Rev. **41**, 7228–7246 (2012)